Journal of Pathology
J Pathol 2014
Published online in Wiley Online Library
(wileyonlinelibrary.com) DOI: 10.1002/path.4360

ORIGINAL PAPER

Mixed-species biofilm compromises wound healing by disrupting epidermal barrier function

Sashwati Roy,[1,3,#] Haytham Elgharably,[1,3,#] Mithun Sinha,[1,3] Kasturi Ganesh,[1,3] Sarah Chaney,[2,5,8] Ethan Mann,[2,5] Christina Miller,[3] Savita Khanna,[3] Valerie K Bergdall,[6] Heather M Powell,[7] Charles H Cook,[3] Gayle M Gordillo,[1,4] Daniel J Wozniak[2,5] and Chandan K Sen[1]*

[1] *Comprehensive Wound Center, Davis Heart and Lung Research Institute, Centers for Regenerative Medicine and Cell Based Therapies, Ohio State University Medical Center, Columbus, OH, USA*
[2] *Microbial Interface Biology, College of Veterinary Medicine, Ohio State University, Columbus, OH, USA*
[3] *Department of Surgery, College of Veterinary Medicine, Ohio State University, Columbus, OH, USA*
[4] *Department of Plastic Surgery, College of Veterinary Medicine, Ohio State University, Columbus, OH, USA*
[5] *Department of Microbial Infection and Immunity, Microbiology, College of Veterinary Medicine, Ohio State University, Columbus, OH, USA*
[6] *Department of Veterinary Preventive Medicine, College of Veterinary Medicine, Ohio State University, Columbus, OH, USA*
[7] *Department of Materials Science and Engineering, College of Veterinary Medicine, Ohio State University, Columbus, OH, USA*
[8] *Department of Veterinary Biosciences, College of Veterinary Medicine, Ohio State University, Columbus, OH, USA*

**Correspondence to: CK Sen, 473 West 12th Avenue, 512 DHLRI, Ohio State University Medical Center, Columbus, OH 43210, USA. E-mail: chandan.sen@osumc.edu*

[#]These authors contributed equally to this study.

Abstract

In chronic wounds, biofilm infects host tissue for extended periods of time. This work establishes the first chronic preclinical model of wound biofilm infection aimed at addressing the long-term host response. Although biofilm-infected wounds did not show marked differences in wound closure, the repaired skin demonstrated compromised barrier function. This observation is clinically significant, because it leads to the notion that even if a biofilm infected wound is closed, as observed visually, it may be complicated by the presence of failed skin, which is likely to be infected and/or further complicated postclosure. Study of the underlying mechanisms recognized for the first time biofilm-inducible miR-146a and miR-106b in the host skin wound-edge tissue. These miRs silenced ZO-1 and ZO-2 to compromise tight junction function, resulting in leaky skin as measured by transepidermal water loss (TEWL). Intervention strategies aimed at inhibiting biofilm-inducible miRNAs may be productive in restoring the barrier function of host skin.

Keywords: wound biofilm; porcine burn wounds; microRNA; transepidermal water loss (TEWL); mixed-species biofilm

Received 18 December 2013; Revised 18 March 2014; Accepted 7 April 2014

No conflicts of interest were declared.

Introduction

In the USA, 6.5 million patients are affected by chronic wounds. The national annual healthcare cost of treating chronic wounds is estimated at US$ 25 billion annually and this burden is rapidly growing, due to increasing health care costs, an ageing population and a sharp rise in the incidence of diabetes and obesity worldwide [1]. Wound infections are not only the most expensive complications following surgery but a major source of bacteria that drive the nosocomial infection rates in hospitals. Bacteria may establish social networks and structurally organize in aggregates known as biofilms. In the biofilm form, bacteria are encased within an extracellular polymeric substance (EPS) and become recalcitrant to antimicrobials and host defences, posing a rapidly escalating threat to human health [2]. Biofilms are estimated to account for 60% of chronic wound infections [3].

Current understanding of wound biofilm biology, including bacterial mechanisms of pathogenesis and host responses, is limited by the availability of appropriate chronic models of wound biofilm infection in which cascading mechanisms may be studied longitudinally over time. Biofilms have been studied for decades under *in vitro* conditions [4]. *In vivo* animal models of biofilm infection have been of short-term acute-phase studies lasting 2–16 days [5–8]. In the case of skin wounds, the porcine model is in agreement with human studies 78% of the time, compared to 53% for the small mammal studies [9]. With respect to translational value, the Wound Healing Society (WHS) recommends the use of the pig as the preclinical model for wound studies

[10]. Preclinical models refer to experimental systems that attempt to most closely mimic a human pathological condition of interest [11]. Wound biofilm has been mostly studied in flies, rodents and rabbits. The porcine model has been also examined, albeit for a short term of 2–7 days following induced infection [12]. Host response to biofilm infection is typically chronic and governed by micro-environmental cues present at the site of infection [13]. Our interest in understanding the host response to chronic infection necessitated the development of a wound infection model that is sustained, in this case for 8 weeks.

Current knowledge supports the notion that the biology of pathological biofilms is driven not only by interactions between different microorganisms at the site of infection but also by bacteria–host interactions, which play a critical role in defining human disease conditions. Thus, we sought to establish a mixed bacterial species biofilm infection (using *Pseudomonas aeruginosa* PAO1 and *Acinetobacter baumannii* 19606) on full-thickness burn wounds. These microorganisms are known to be associated with battle burn wound casualties [14], contributing to chronicity [15]. This novel experimental system led to the observation that, although the effects of chronic biofilm infection on wound closure may be marginal over a period of 2 months, such an infection results in failure of the skin barrier function at the site of healing. While the wound appears closed by visual assessment, the current standard of care, high epidermal water loss resulting from malfunctioning tight junctions, was identified at the site of biofilm infection. Interestingly, this effect was only evident after a month of biofilm infection, i.e. when the wound had achieved chronicity [16]. This work reports the first evidence of biofilm-inducible microRNAs that specifically silence tight junction proteins. Observations in this study underscore the clinical need to utilize objective measures of skin function when evaluating healing outcomes of biofilm-infected wounds.

Materials and methods

Ethics

All animal (mouse and pig) experiments were approved by the Ohio State University Institutional Laboratory Animal Care and Use Committee (ILACUC) under protocols 2008A0012-R1 (pig) and 2009A0214-R1 (mouse).

Bacterial isolates

Pseudomonas aeruginosa strain PAO1 [17], with constitutive expression of GFP, was obtained from the Mathew Parsek laboratory, and *Pseudomonas aeruginosa* strain Δpsl PAO1 were grown on *Pseudomonas* Isolation Agar (PIA) plates or Luria broth without sodium chloride (LBNS) at 37°C. *Acinetobacter baumannii* strain 19606 with spontaneous rifampicin mutation was grown on Luria agar (LA) plates with 100 μg/ml rifampicin or LBNS at 37°C.

Porcine full-thickness burns and bacterial inoculation

A total of 64 domestic Yorkshire pigs were used in this study (for procedural description, see supplementary material, Supplementary materials and methods).

Histology and imaging

Histopathology was performed as described [18]. In brief, formalin-fixed paraffin-embedded wound sections were deparaffinized and stained with haematoxylin and eosin (H&E), Masson's trichrome and Gram/Twort stain (Newcomer Supply Inc.), using standard procedures. Immunohistochemical staining of OCT-embedded frozen sections were performed as described previously [18], using the following primary antibodies: anti-*Pseudomonas* antibody (custom developed by Covance, Denver, PA, USA), anti-*Acinetobacter* antibody (custom developed by Covance) and ZO-1 and ZO-2 (Invitrogen). Because of the high autofluorescence in porcine tissue and weak GFP signal emitted from our PAO1::*gfp* strain, we chose to visualize *P. aeruginosa* with anti-*Pseudomonas* antibody rather than relying on the GFP signal. Mosaic images were collected using a Zeiss Axiovert 200 inverted fluorescence microscope, supported by an AxioCam digital camera and a motorized stage and guided by Axiovision software (Zeiss). Each mosaic image was generated by combining a minimum of 100 images. Confocal laser-scanning microscopy (CLSM) was performed using a Fluoview FV1000 spectral confocal microscope (Olympus, Pittsburgh, PA, USA) equipped with an argon laser. Z-stack images were created by merging serial scans of tissue sections (20–50 μm).

Scanning electron microscope imaging

Samples processing and imaging was performed as described [19]. In brief, following glutaraldehyde fixation and dehydration with a graded series of ethanol, the samples were treated with hexamethyldisilazane (HMDS; Ted Pella Inc.) and left overnight to dry. Before scanning, the samples were mounted and coated with gold. Imaging of the samples was done using a FEI™ NOVA nanoSEM scanning electron microscope (FEI™, Hillsboro, OR, USA) equipped with a field-emission gun electron source.

Surgical debridement and laser Doppler blood flow imaging

Debridement was performed using a 0.12 inch Weck blade to remove necrotic and infected tissues until bleeding healthy tissue was exposed. Debridement was performed according to the standard of care in a clinical setting. The MoorLDI-Mark 2 laser Doppler blood perfusion imager (Moor Instruments Ltd, UK)

was used to map tissue blood flow in debrided wounds, as described previously [18].

Transepidermal water loss (TEWL)

DermaLab TEWL Probe (cyberDERM inc., Broomall, PA) was used to measure TEWL from the wounds, expressed in g/m^2/h.

Laser-capture microdissection (LCM) and biofilm gene expression analysis

Serial sections were obtained from OCT-embedded frozen wound sections; one of the serial sections was stained with anti-*Pseudomonas* antibody, as described earlier, for visualization of the biofilm-infected area. Other serial sections (10 μm) were stained using a modified haematoxylin QS procedure. The sections were mounted on polyethylene napthalate (PEN) membrane glass slides (P.A.L.M. Microlaser Technologies AG, Germany) that had been RNAsin (Ambion)- and UV-treated, for cutting and catapulting, as described by our group [20]. Corresponding *P. aeruginosa*-stained areas were captured in chaotropic RNA lysis solution [20]. The RNA was extracted using a TRIzol® Max™ Bacterial RNA Isolation Kit (Life Technologies) according to the manufacturer's instructions. Reverse transcription and mRNA quantitation using real-time PCR were performed as described [20].

Cell culture and transfection

Human immortalized keratinocytes (HaCaT) were grown under standard culture conditions (at 37°C in a humidified atmosphere consisting of 95% air and 5% CO_2) in Dulbecco's modified Eagle's medium (DMEM) supplemented with 10% FBS, 100 IU/ml penicillin, 0.1 mg/ml streptomycin, 10 mM L-glutamine, as described previously [21].

In vitro static biofilm co-culture

Bacterial biofilms were grown on HaCaT cells using a co-culture model system adapted from Anderson *et al* [22]. In brief, the confluent cultures of HaCaT cells were inoculated with bacterial cultures of *P. aeruginosa* (10^5 CFU/ml) and *A. baumannii* (10^6 CFU/ml) in antibiotic-free culture medium. The plates were incubated for 1 h at 37°C and 5% CO_2, **a**fter which the supernatant was replaced with fresh DMEM (without antibiotics) supplemented with 0.4% arginine. *In vitro* biofilm culture on a polycarbonate membrane was adapted from Zhao *et al* [23]. The cells were further incubated under regular culture conditions for specified times as described in the figures.

Western blot analyses

Western blot was performed using antibodies against ZO1 (Invitrogen), ZO2 (Invitrogen) and β-actin (Sigma), as described previously [21].

RNA isolation and quantitative real-time PCR

Total RNA, including the miRNA fraction, was isolated using a *mir*Vana miRNA isolation kit (Ambion), according to the manufacturer's protocol. Specific Taqman assays for miRNA (Applied Biosystems) and a *mir*Vana qRT–PCR miRNA RT Kit (Applied Biosystems) were used with a real-time PCR system and Taqman Universal Master Mix. Levels of miRNA were quantified using the relative quantification method, using *U6* small nuclear RNA as the housekeeping factor. The transcription levels of ZO1 and ZO2 and housekeeping control GAPDH were quantified using SYBR green I (Applied Biosystems). Expression levels of miRNA and mRNA were quantified by employing the $2^{-\Delta\Delta CT}$ relative quantification method [21] (for primer sequences, see supplementary material, Supplementary materials and methods).

miR-Target 3′-UTR luciferase reporter assay

miRIDIAN mimic-miR-146a or -106b were transfected to HaCaT cells, followed by transfection with pmiR Target-ZO-1-3′-UTR or pmiR Target-ZO-2-3′-UTR plasmids. Luciferase assays were performed using the dual luciferase reporter assay system (Promega), as described. Normalization was achieved by co-transfection with *Renilla* plasmid [24]. Data are presented as the ratio of firefly:*Renilla* luciferases.

Immunocytochemistry

Cells were fixed with IC fixation buffer (eBioscience), blocked and incubated with primary antibody against ZO1 (1:100) or ZO2 (1:100) overnight at 4°C. Signal was visualized using FITC-tagged α-rabbit (1:200; Invitrogen) and counterstained with DAPI (1:10 000; Invitrogen) [25].

miR mimic delivery on mice skin

Male C57BL/6 mice (aged 8 weeks) were used. miRNA mimics, 3 μg/5 μl (miR-146a mimic, miR-106b mimic and non-targeting miRNA mimic *Coenorhabditis elegans* miR-67 as negative control; Dharmacon) were incubated with 5 μl siPort transfection reagent (Ambion) for 30 min and mixed with 10 μl cream (composition of the cream was as described [26]). The miRNA mix was rubbed onto a marked (8 × 16 mm^2) and depilated dorsal area. The mimics were applied daily for a period of 10 days. Before the application of the miRNA mimics, TEWL measurements of the mouse skin were taken using Dermalab Series Skinlab Combo (Cortex Technologies). The animals were sacrificed at day 11 and the skin where the mimic was applied was harvested. All the animal studies were performed in accordance with protocols approved by the Laboratory Animal Care and Use Committee of Ohio State University.

Statistics

In vitro data are reported as mean ± standard deviation (SD) of three to six experiments, as indicated in the

respective figure legends. Comparisons among multiple groups were tested using analysis of variance (ANOVA); $p < 0.05$ was considered statistically significant. For animal studies, data are reported as mean ± SD of at least three or four animals, as indicated. Given the small sample size, Mann–Whitney or Kruskal–Wallis one-way ANOVA tests were performed to test the significance ($p < 0.05$) of differences between means.

Results

Establishment and characterization of the mixed-species, full-thickness wound biofilm model

The first objective of this study was to develop a preclinical, large animal model that would further our understanding of the underlying impaired host tissue responses implicated in the healing of biofilm-infected burn wounds. We developed a microprocessor-controlled, electrically heated burning device to create uniform, full-thickness thermal injuries of a defined size and depth (see supplementary material, Figure S1). A mixed bacterial species infection approach was adopted, combining *Acinetobacter baumannii* 19606 and *Pseudomonas aeruginosa* PAO1 to co-infect burn wounds and establish a clinically relevant mixed-species biofilm infection (Figure 1). These microorganisms are highly relevant, as they are typically associated with battle burn wound casualties [14]. Following induced infection (group II, representing clinically infected wounds; spontaneously infected wounds, or the SI group, served as controls; see Methods), inspection of the wounds revealed yellowish-green discoloration with a discharge that increased with time (Figure 1A). Histological and microbiological analyses confirmed bacterial colonization of the wound bed (Figure 1C). Direct microscopic visualization of *A. baumannii* and *P. aeruginosa* colonies revealed the presence of both organisms in burn wounds 7 days postinoculation. Occasionally, co-localization of both organisms in the wound bed was noted, supporting the establishment of mixed-species biofilm infection (Figure 1D). Imaging of burn wound biopsies with scanning electron microscopy (SEM) demonstrated aggregates of bacteria attached to the surface of the burn wounds that were embedded in an EPS, indicating a biofilm matrix (Figure 1B) similar to that in clinical pressure ulcer wound SEM micrographs (Figure 1E). Thus, our newly developed preclinical mixed-infection biofilm model replicates key histological characteristics when compared to human clinical chronic wound samples.

In addition to bacteria embedded in EPS, the criteria for defining biofilm infection include: (1) adherence to a surface or each other; (2) persistent and localized infection; and (3) resistance to antimicrobial treatments [27]. Data that support these criteria are indicated here:

1. *Adherence to surface*. A scrubbing technique was used to test the adherence of the biofilms to the wound surfaces [12,28]. This technique is known to remove free (planktonic) bacteria from burn wounds. Scrubbing was performed with double, open-ended, sterile, plastic tubes; sterile saline was added thrice, followed by once with a detergent (4% Tween 80 v/v). Microbiological analyses revealed that bacterial counts did not change significantly before or after scrubbing, suggesting strong bacterial adherence to the wound (not shown). This, combined with direct visualization of the biofilms by SEM and confocal microscopy (Figure 1), support this criterion.
2. *Persistent and localized infection*. Bacterial infection was present in the burn wounds until days 14 and 35 post-inoculation, indicating persistence (see supplementary material, Figure S2). Localized infection was established with negative blood cultures and lack of systemic signs of infection (data not shown).
3. *Resistance to anti-microbial treatments.* Silver dressing Acticoat 7™ represents the standard of care for the management of infected wounds [29]. *In vitro*, incubation of Acticoat 7™ with planktonic cultures of *A. baumannii* and *P. aeruginosa* effectively eradicated both bacterial species (Figure 2A). However, Acticoat 7™ dressing was ineffective against bacterial biofilms in burn wounds (Figure 2B, C).

Mixed-species wound biofilm is resistant to debridement

Debridement of the biofilm infected burn wound was performed by a plastic surgeon wound care specialist, using a Weck blade to remove necrotic and infected tissues until bleeding healthy tissue was exposed, as documented using Doppler blood flow analysis (Figure 2D, F, G). CFU analyses revealed significant but transient lowering of bacterial burden following debridement. However, the *P. aeruginosa* bacterial burden was restored to almost the initial levels within 48 h, demonstrating that debridement alone was not effective to eradicate biofilm infection (Figure 2E). IHC staining of *A. baumannii* and *P. aeruginosa* indicated microcolonies of both bacteria in deeper tissue of the debrided wound bed, cautioning that debridement may actually promote deep tissue infection (Figure 2H).

Induction of biofilm-specific genes in infected wound-tissue elements

It is well established that in a sessile biofilm lifestyle, bacteria acquire unique phenotypes by modulating gene expression that supports biofilm biology [30]. While there is no known 'biofilm biomarker gene' identified for *P. aeruginosa*, we evaluated the expression patterns of some genes previously studied under biofilm growth conditions. These included *rpoS,* which is implicated in the morphology and antibiotic resistance of biofilms [30], and *rhlR*/*aprA*, previously linked to quorum sensing and biofilms [31,32]. The expression of *rhlR, rpoS* and *arpR* were significantly up-regulated in biofilm

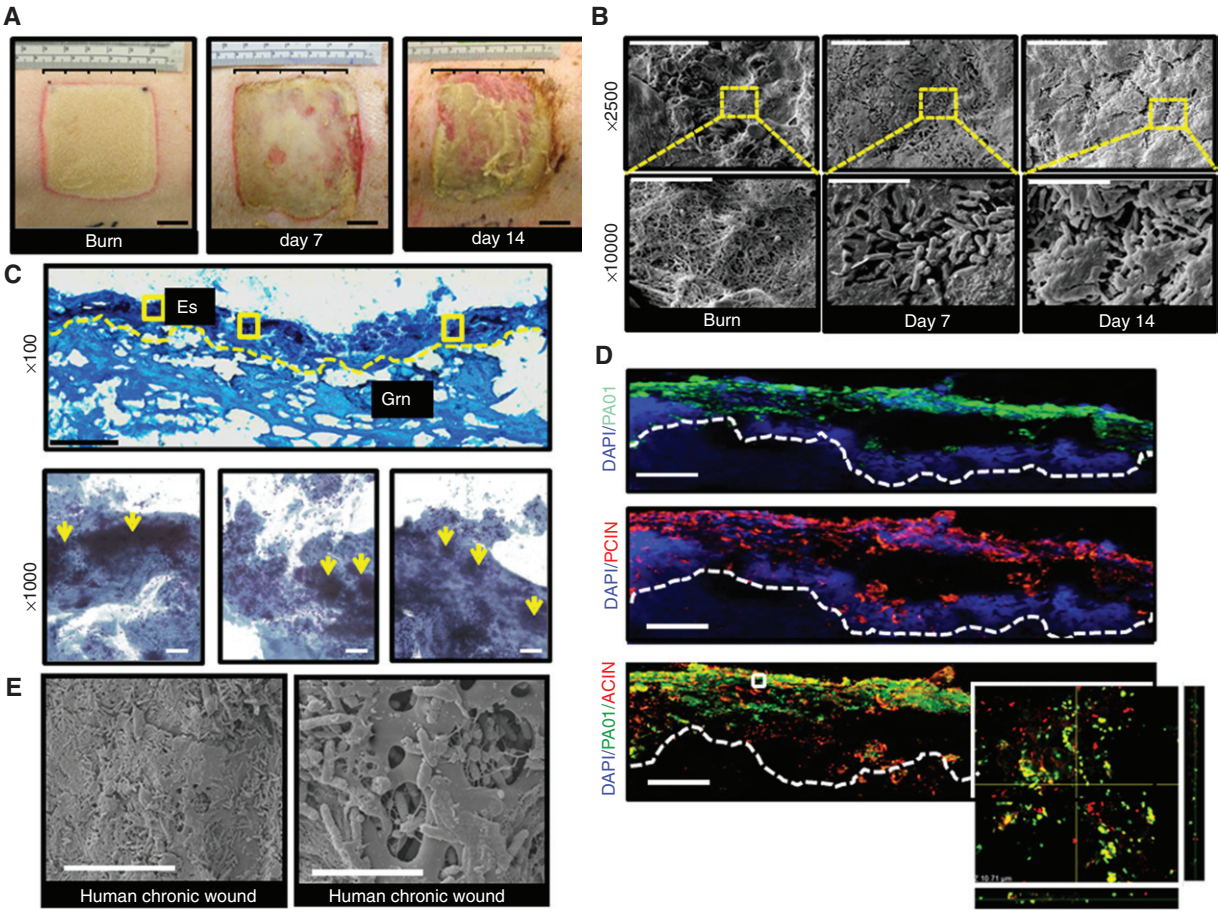

Figure 1. Establishment of mixed-species biofilm infection in a full-thickness porcine burn wound model. Six 2 × 2 in^2 burn wounds were created with a burning device (see supplementary material, Figure S1). Co-infection of the burn wounds was performed on day 3 post-burn with *P. aeruginosa* PA01 and *A. baumannii 19606*. (A) Representative digital photograph of wounds on the day of burning, days 7 and 14 post-infection. Note signs of active infection, with localized erythema, yellowish exudates and friable wound edges on days 7 and 14 post-infection. (B) Scanning electron microscope (SEM) images of biopsies collected from the wounds on the day of burning and days 7 and 14 post-infection. The images clearly demonstrate a mixture of extracellular tissue matrix, fibres and red blood cells over the surface of burn wounds before bacterial inoculation. Large aggregates of rods attached to the wound surface, encased in a layer of extracellular amorphous material, were noted on days 7 and 14 post-infection; (upper panel) scale bar = 20 μm, ×2500 magnification; (lower panel) magnification of the red dashed boxes in the upper panels; scale bar = 5 μm, ×10 000 magnification. (C) Gram-stained images of inoculated wounds shows presence of bacterial aggregates: (upper panel) representative mosaic image of a day 7 post-infection wound; images collected under ×400 magnification using microscope supported with a motorized stage; scale bar = 200 μm; Es, eschar; Grn, granulation tissue: (lower panels) zoom of three-boxed area in upper panel image showing Gram-negative bacilli and coccobacilli over the surface of the burn wound, while large Gram-negative clumps colonize the wound tissues (yellow arrows); scale bar = 50 μm. (D) Both *P. aeruginosa* and *A. baumannii* on the burn wounds were visualized using anti-*Pseudomonas* (green) and anti-*Acinetobacter* (red) antibody and confocal laser-scanning (CLSM) microscopy. Merged (red and green) immunofluorescence images of day 7 (post-infection) wound biopsies show heavy colonization of wound tissues with both strains. Mosaic images were collected under ×400 magnification, using a fluorescent microscope supported by a motorized stage; scale bar = 100 μm. Z-stack images of boxed areas of the lower panel surface of burn wound tissues. (Inset) Zoom of the boxed area in merged image. The image was created by merging serial scans of a thick tissue section (20 μm), viewed under ×600 magnification in a CLSM. Dense microcolonies of *P. aeruginosa* and *A. baumannii* were noted, with some co-localization in the wound tissues. The *x*–*z* and *y*–*z* planes display the thickness of the microbial clumps within the tissue section. (E) Representative SEM image of wound biopsies from human chronic pressure ulcers, showing that the bacterial colonization and biofilm established in the experimental porcine biofilm model is comparable to that of human chronic wounds: (left panel) scale bar = 20 μm, ×2500 magnification; (right panel) scale bar = 5 μm, ×10 000 magnification

bacteria laser-captured from burn wounds compared to those of planktonic bacteria obtained from wound-scrub fluid (Figure 3A–C). These observations further support biofilm formation in the model reported here.

Biofilm infections compromise skin barrier function

Development of the wound biofilm model was aimed at elucidating novel aspects of the host response that may only be studied in a long-term experimental system. For the purposes of studying the host response to induced biofilm formation, controls were considered burn wounds not exposed to bacterial inoculation (sterile, PBS mock-inoculated). Despite standard wound care management, control wounds occasionally developed spontaneous infection from the skin microflora. During a long-term experimentation setting we observed that inoculation of some wounds on a pig resulted in

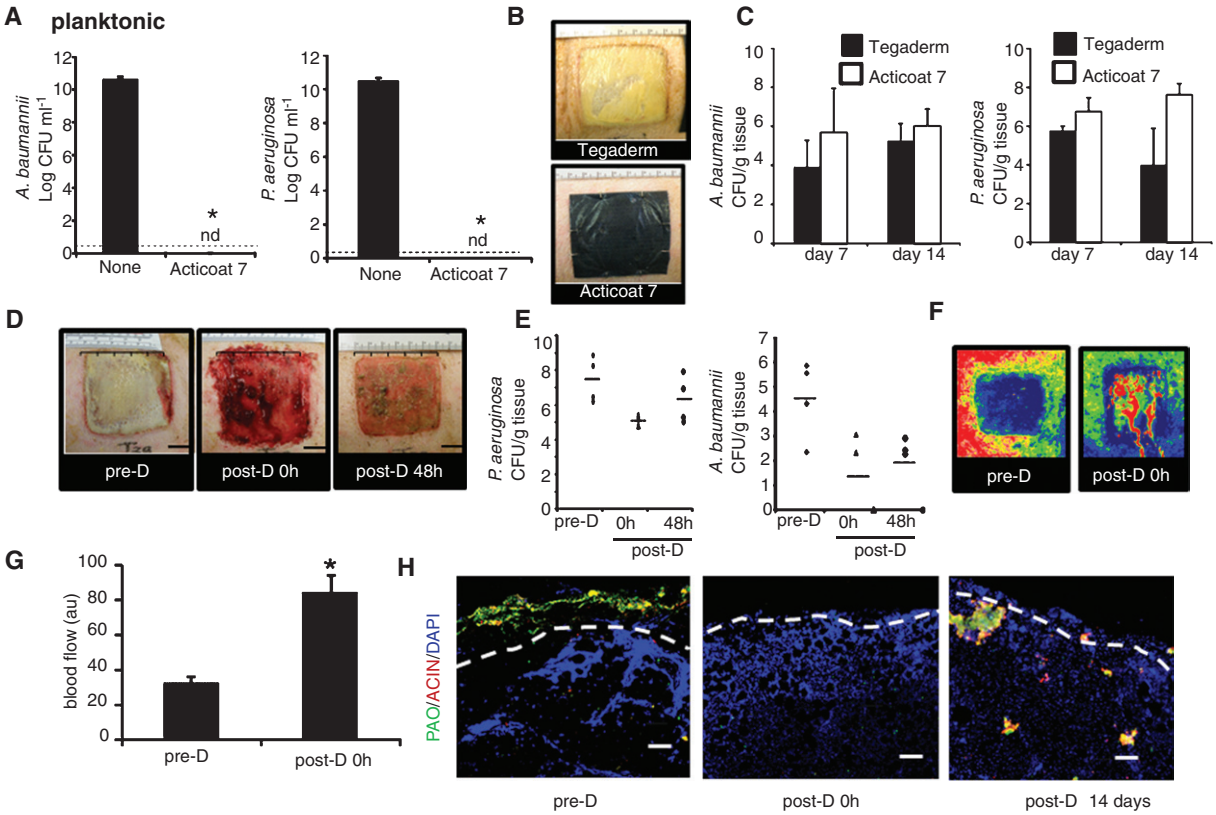

Figure 2. Resistance of mixed-species biofilm to antimicrobial and debridement. (A–C) Antimicrobial Acticoat 7™ effectively kills bacteria in the planktonic phase, while ineffective against wound biofilm. (A) Planktonic cultures of *P. aeruginosa* and *A. baumannii* were incubated in the presence or absence of Acticoat 7™ for 24 h, followed by determination of bacterial CFU. The treatment was highly effective in killing the bacteria: nd, not detectable; data are mean ± SD ($n = 4$); $^{*}p < 0.05$. (B) Images of wounds covered with Tegaderm™ or Acticoat 7™. (C) Microbiological analysis of porcine burn wounds covered with Tegaderm™ or Acticoat 7™ on days 7 or 14 postinoculation; Acticoat 7™ was ineffective in attenuating any bacterial load from wounds, suggesting that the bacteria in the biofilm were resistant to antimicrobial treatment; data are mean ± SD; $n = 3$. (D–H) Debridement was performed using a 0.12 inch Weck blade, by removing necrotic and infected tissues until bleeding healthy tissue was exposed. (D) Digital images of burn wound predebridement (pre-D), immediately post-debridement (post-D, 0 h) or 48 h (post-D, 48 h) after debridement. (E) Microbiological analysis revealed a significant decrease in bacterial burden after debridement. The bacterial burden for *P. aeruginosa* was restored to almost to the initial level 48 h post-D, suggesting that debridement alone does not eradicate biofilm; data are mean ± SD; $^{*}p < 0.05$ ($n = 3$). (F) Laser Doppler imaging was performed to demonstrate that there was no blood flow (blue) in predebrided burn wounds, while the healthy, well-perfused (red) tissue is exposed immediately after debridement. (G) Bar graph represents quantitation of the laser Doppler blood flow imaging. (H) Immunohistochemical staining of *P. aeruginosa* (green) and *A. baumannii* (red) burn wounds following debridement demonstrate that the bacterial biofilm (microcolonies) are restored in deeper layers of the wounds on day 14 post-debridement. White dashed line, line of debridement; scale bar = 100 μm

colonization of all wounds by the inoculated bacteria. Thus, pigs bearing control wounds were separately housed and wholly dedicated for that purpose. In the current standard of clinical care, wound closure is determined based on visual inspection by the wound care physician. Closure, as appreciated by visual inspection, of biofilm infected wounds was comparable to that of non-inoculated control wounds (Figure 4A, B). When skin is injured its barrier function is impaired, resulting in higher transepidermal water loss (TEWL), an index to assess skin barrier function *in vivo* [33]. Therefore, in addition to visual documentation of wound closure, a TEWL assay was performed to quantitatively determine the re-establishment of skin barrier function following burn wounds. Interestingly, although visual wound closure was unaffected by biofilm infection, marked impairment in the restoration of skin barrier function was noted in biofilm-infected wounds compared to non-inoculated control wounds (Figure 4C).

Silencing of tight junction proteins by biofilm infection

The barrier function of the skin is maintained by integrity of adhesive interaction at the epithelial apical junction complex, comprised mainly of tight junctions, adherens junctions, desmosomes and gap junction proteins [34]. Zona occludens-1 (ZO-1) and zona occludens-2 (ZO-2) represent two key tight junction proteins that were found to be significantly down-regulated in biofilm infected burn wounds (Figure 5A; see also supplementary material, Figure S3).

Biofilm-inducible cutaneous miRNA silences ZO-1 and ZO-2 and increases TEWL

In our search for mechanisms silencing ZO-1 and ZO-2, bioinformatic analyses recognized miR-146a and miR-106b with potential binding sites on ZO-1 and ZO-2 mRNA (see supplementary material, Figure S4).

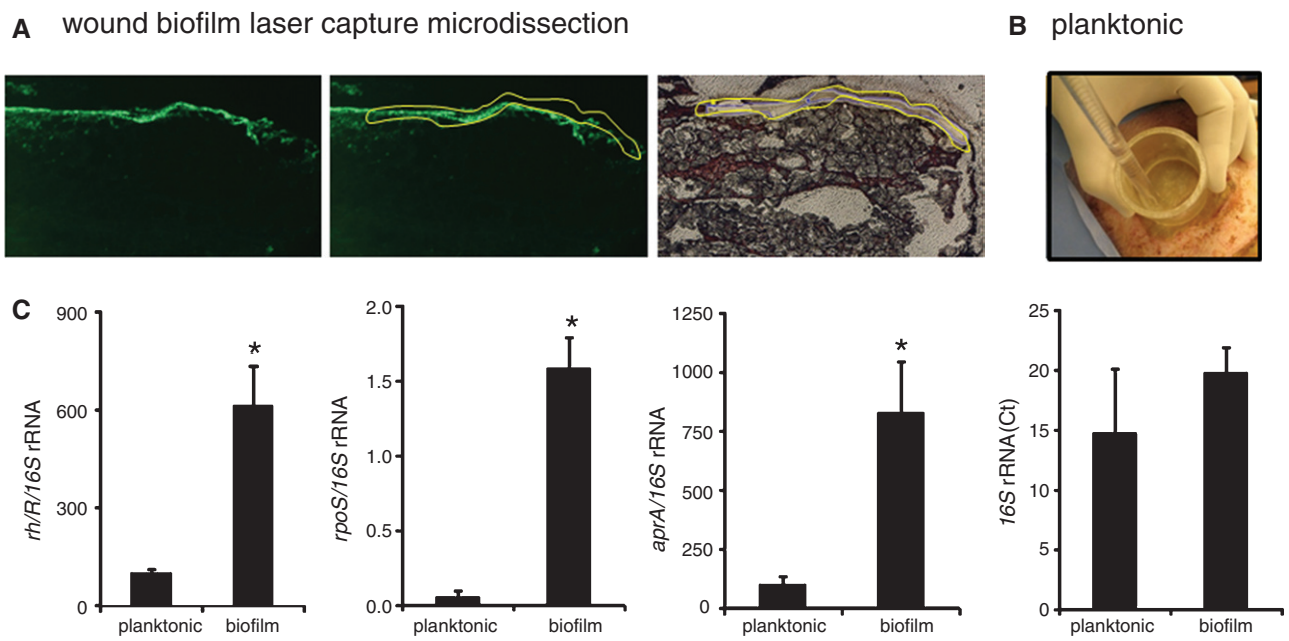

Figure 3. Abundant expression of biofilm-specific genes in biofilm tissue elements, captured using LCM. (A) Frozen serial sections (10 μm) from biofilm-infected wound tissue were stained with anti-PAO1 (green) antibody. The next serial sections were stained with haematoxylin to visualize the corresponding biofilm-affected area. Images are representative: (left) anti-PAO1 stained image; (middle) anti-PAO1-stained tissue marked to delineate the biofilm affected area; and (right) the area of biofilm was cut/captured using laser capture microdissection (LCM) from the corresponding haematoxylin-stained section. (B) To collect planktonic bacteria from wounds, a sterile double open-ended plastic tube was placed on a wound, followed by washing once with 4 ml PBS. The wash suspension was collected and spun down to retrieve bacterial pellets. This procedure results in removal of loosely adhered or planktonic forms of bacteria. (C) LCM-captured tissue was used for quantification of mRNA levels of biofilm-specific mRNA, using real-time PCR and normalized against *16S* rRNA expression. *16S* rRNA levels have been presented to demonstrate comparable levels in both plankonic and captured biofilm groups; data are mean ± SD ($n = 4$); $^{*}p < 0.05$ compared to planktonic

Interestingly, expression of miR-146a and miR-106b were significantly induced in response to biofilm infection of wounds when compared with uninfected controls (Figure 5B). Does biofilm infection indeed induce miR-146a and miR-106b? Are ZO-1 and ZO-2 biologically validated targets of miR-146a and miR-106b? To answer these two questions, we relied on an *in vitro* model involving static biofilms grown on human keratinocyte monolayers [22]. Exposure of keratinocytes to mixed-species biofilm silenced ZO-1/ZO-2 (Figure 6A) and induced miR-146a/miR-106b (Figure 6B), consistent with *in vivo* findings (Figure 5). While *Pseudomonas* monospecies biofilm induced both miR-146a and miR-106b, *Acenitobacter* biofilm induced miR-106b but not miR-146a. Biofilm featuring the co-presence of *Pseudomonas* and *Acenitobacter* demonstrated an additive effect in inducing miR-106b (Figure 6B). The use of the Δpsl poor biofilm-producing strain of *P. aeruginosa* PAO1 failed to induce both miRs, pointing towards the significance of biofilm infection in inducing miR-106b and miR-146a (Figure 6C). The observation that conditioned media from biofilm cultures, not planktonic cultures, were able to induce miR-146a and miR-106b indicate that the miR regulatory factor may be secreted (Figure 6D).

To directly connect these miRs to ZO-1/ZO-2, immunocytochemical studies using miRidian miR-146a and miR-106b mimics were performed (Figure 6E; see also supplementary material, Figure S5). Transfection with hsa-miR-146a or hsa-miR-106b mimics or their corresponding inhibitors showed that both miRNAs were inversely associated with expression of the corresponding ZO proteins (Figure 6F, G, I). Using ZO-1 3′-UTR and ZO-2 3′-UTR firefly luciferase expression constructs, the effect of the said miRs on ZO transcription was tested (Figure 6H).

Findings of this work show that ZO-1 and ZO-2 are direct targets of miR-146a. While miR-106b expression is co-regulated with ZO-1/ZO-2, these proteins are only targeted by miR146a (Figure 6H). Finally, to determine whether miR-146a and miR-106b may directly influence skin barrier function, miR-146a mimic, miR-106b mimic and non-targeting miRNA mimic were delivered to the dorsal skin of mice via a cream-based vehicle. Delivery of miR mimics silenced ZO-1 and ZO-2 expression and compromised skin barrier function, as manifested by increased TEWL (Figure 7A–C; see also supplementary material, Figure S6).

Discussion

The skin is the largest organ of the human body, which provides an effective barrier between the organism and the environment. When the barrier is breached, as in chronic wounds, biofilms are often present in the host tissue for extended periods, during which time they may compromise the host response to injury. Presence

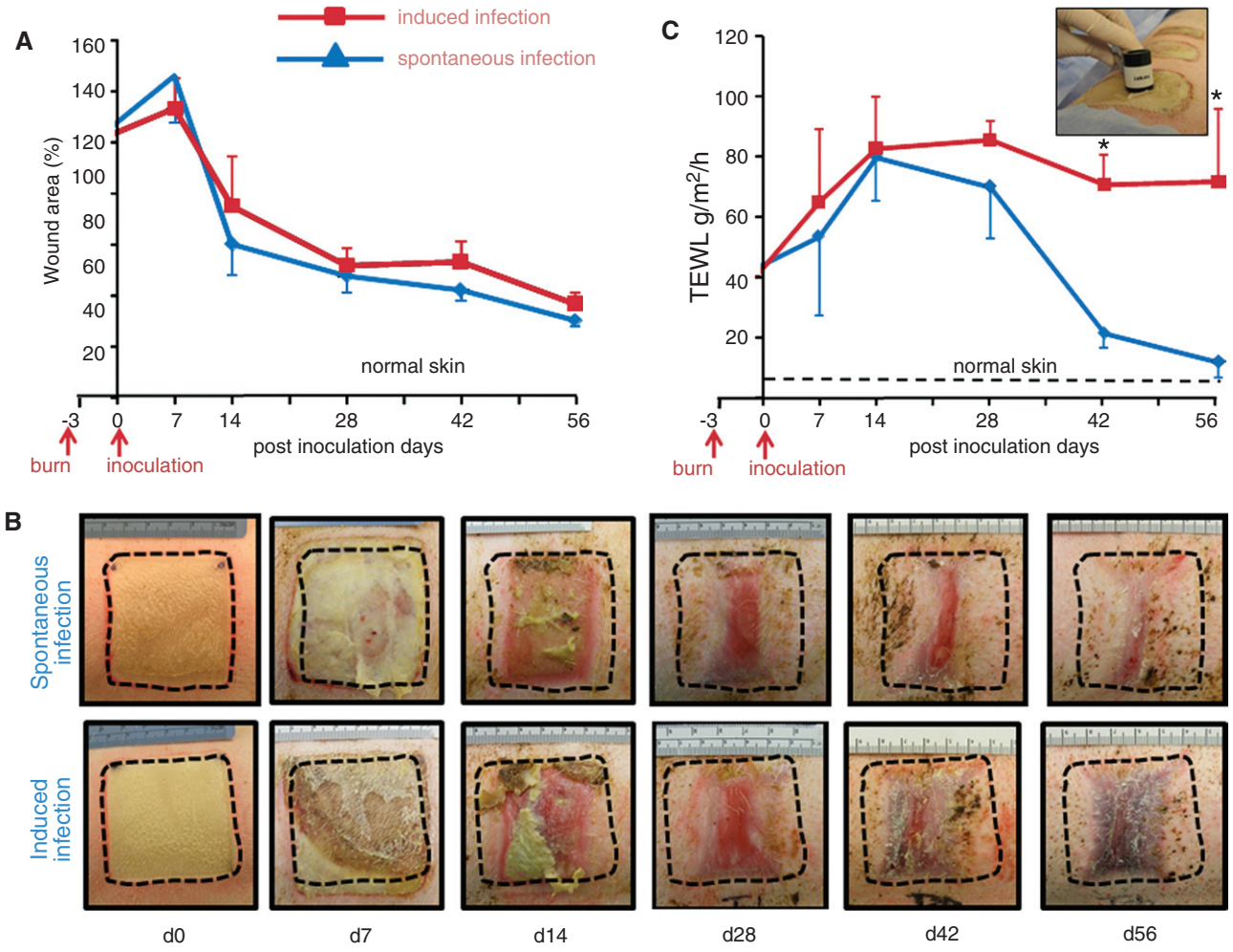

Figure 4. Biofilms infection compromised re-establishment of skin barrier function. (A) Wound closure in spontaneous infection (blue line, control) or induced infection (red line) wounds; data are presented as percentage of the initial wound area, mean ± SD ($n = 4$). (B) Representative digital images from spontaneous infection or induced infection wounds burn wounds. (C) Transepidermal water loss (TEWL) analysis from spontaneous infection and induced-infection burn wounds; (inset) DermaLab TEWL probe used for the measurement of the transepidermal water loss from the wounds; TEWL expressed in g/m^2/h; data are mean ± SD ($n = 4$); $^*p < 0.05$ compared to spontaneous infection

of biofilm has been reported in ischaemic wounds, including burns [35,36]. The pig is widely acknowledged as the animal of choice to serve as a preclinical model of skin wound healing [9,18]. At present, all experimental systems addressing skin wound biofilms in pigs are short in duration and therefore inadequate to understand the long-term, clinically relevant host responses to wound biofilms [12,37]. This is the first study of mechanisms underlying the wound biofilm over an 8 week period. The burn wound biofilm developed herein satisfied the criteria for an established biofilm by being surface-adherent, persistent and localized over 4 weeks, and resistant to silver dressings and debridement, which are used as a standard of care in managing infected wounds. We found that debridement promoted deep-tissue colonization of bacterial biofilms; although colonization of bacteria to deeper tissue had been reported [38], no clear evidence was provided linking debridement with deep tissue infection.

TEWL is a reliable measure of skin barrier function [33]. The nucleated epidermis contributes to this barrier primarily via tight, gap and adherens junctions. The absence of the tight junction proteins [39] in mice results in lethal skin-barrier function failure [40]. ZO proteins are ubiquitous scaffolding proteins that enable assembly of multiprotein complexes at the cytoplasmic surface of the plasma membrane and link transmembrane proteins to the filamentous cytoskeleton. ZO-1 acts as a scaffolding molecule during the formation of junctional complexes, such as tight junctions, gap junctions and adherens junctions [41]. ZO-2 is present at the tight junction of epithelial cells regulating barrier function [42]. Both ZO-1- and ZO-2-deficient mice are embryonic lethal [43,44]. ZO-2-deficient mice show overt signs of epithelial barrier defect, leading to death [44]. Bacteria are known to perturb tight junctions. Several bacterial pathogens actively spread within human tissues by the pathogen-induced recruitment of host filamentous (F)-actin. F-actin forms a tail behind the microbe, propelling it through the cytoplasm and compromising tight junction function [45]. Specifically, *P. aeruginosa* type III-secreted toxins disrupt the

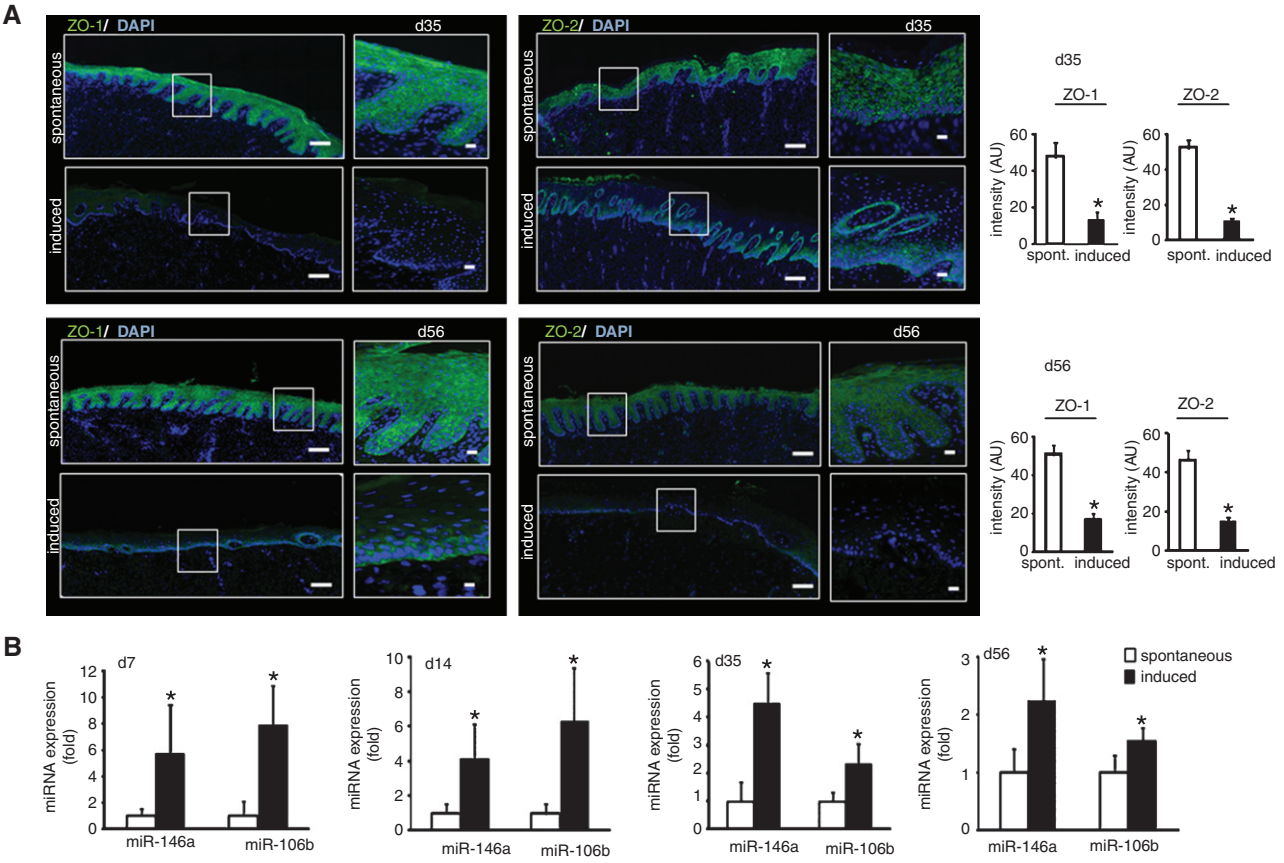

Figure 5. Silencing of tight junction proteins by biofilm infection. Wound biopsies were collected at specified time points after inoculation from spontaneous infected (spont, no inoculation, control) or induced infected (induced), inoculated with *A. baumannii* and *P. aeruginosa*. (A) Representative mosaic (scale bar = 200 μm) and corresponding zoomed (scale bar = 50 μm) images of ZO-1- and ZO-2-stained sections on days 35 and 56 postinoculation, demonstrating reduced expression of the proteins following induced infection; OCT-embedded frozen sections (10 μm), stained using anti-ZO-1 (green) or anti-ZO-2 (green). The sections were counterstained using DAPI. Bar graphs present quantitation of ZO-1 and ZO-2 signal intensity; data are presented as mean ± SD ($n = 3$), $^{*}p < 0.05$ compared to spontaneous. (B) Expression of miR-146a and miR-106b in wound biopsies collected on days 7–35 postinoculation from spontaneous or induced burn wounds; data presented as mean ± SD ($n = 3$); $^{*}p < 0.05$ compared to spontaneous infection

epithelial barrier in the lung by down-regulating tight junction proteins, including ZO-1 [46]. Consistent with these observations, this study presents the first evidence demonstrating that skin barrier function is compromised by mixed-species biofilm infection. Primary targets in such pathology are ZO-1 and ZO-2, both of which are significantly down-regulated in response to biofilm infection. This observation has outstanding clinical significance because it raises the possibility that, although biofilm-infected wounds may visually appear to be closed, the current standard for clinical care, they may actually be open because of the presence of functionally compromised leaky skin.

miRNAs regulate epithelial barrier function. Gene ablation of *Dicer1* demonstrated that miRNAs play a vital role in the differentiation and function of the intestinal epithelium [47]. Specifically, TNFα regulates intestinal permeability by inducing miR-122a-mediated degradation of occludin mRNA [48]. More recently, over-expression of miR-21 in patients with ulcerative colitis has been shown to impair intestinal epithelial barrier function through targeting the Rho GTPase RhoB [49]. None of these mechanisms implicate miR-dependent silencing of ZO proteins in compromising epithelial barrier function in any tissue system. As of now, the only miR known to directly silence ZO proteins is miR-212 [50]. The current study validates both ZO-1 and ZO-2 as direct targets of miR-146a, which is induced in skin in response to inflammation [51]. In addition, miR-146a expression is elevated by microenvironmental signals in the epidermis, rendering Langerhans cells less susceptible to inappropriate activation by commensal bacteria, triggering TLR2 [52]. In the skin, miR-146a may also function as a negative regulator of TGFβ1-induced myofibroblast transdifferentiation by targeting SMAD4 [53]. In non-infected murine diabetic wounds, low expression of injury-inducible miR-146a is claimed to be responsible for impaired wound healing [54]. The current report presents the first evidence demonstrating that biofilm infection may induce miRNAs in the host tissue. Both miR-146a and miR-106b were recognized as being biofilm-inducible in the skin. Although the 3′-UTR regions of ZO-1 and ZO-2 were recognized to be direct targets of miR-146a, that was not the case for miR-106b. miR-106b did not target the 3′-UTR region

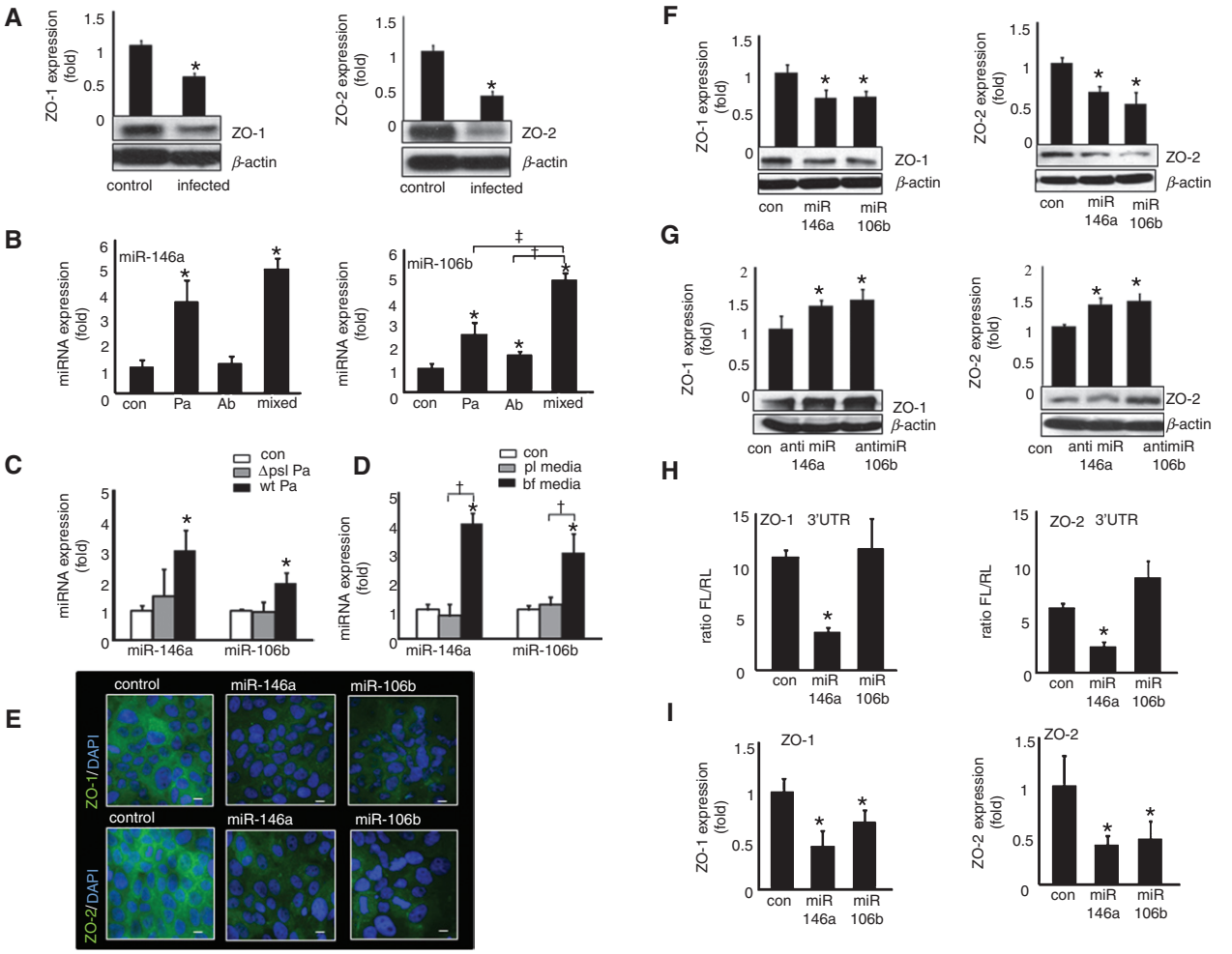

Figure 6. Biofilm-inducible miRNA silences ZO-1 and ZO-2. Human keratinocyte (HaCaT) cells were infected with a static biofilm infection, as described in Materials and methods. (A) Western blot of ZO-1 and ZO-2 expression following 12 h of infection, as compared to non-infected cells (control); data are mean ± SD ($n = 3$); $^{*}p < 0.05$ compared to control. (B) Expression of miR-146a and miR-106b in keratinocytes following 12 h of *P. aeruginosa* PAO1 (Pa), *A. baumannii* 19606 (Ab) mixed (both Pa and Ab) infection compared to non-infected control; data represented as mean ± SD ($n = 4$); $^{*}p < 0.05$ compared to control; $^{\dagger}p < 0.05$ compared to *A. baumannii* and $^{\ddagger}p < 0.05$ compared to *P. aeruginosa*. (C) Expression of miR-146a and miR-106b in keratinocytes following 12 h of poor biofilm-forming *P. aeruginosa* Δpsl PAO1 (Pa), wild-type biofilm-forming *P. aeruginosa* PAO1 (Pa) infection, compared to non-infected control; data represented as mean ± SD ($n = 4$); $^{*}p < 0.05$ compared to control. (D) Expression of miR-146a and miR-106b in keratinocytes following 12 h of incubation with planktonic bacterial medium and biofilm bacterial medium compared to non-infected control medium; data represented as mean ± SD ($n = 4$); $^{*}p < 0.05$ compared to control medium and $^{\dagger}p < 0.05$ compared to planktonic control medium. (E) Human keratinocytes were transfected with miR-146a a miR-106b mimics for 48 h, followed by immunocytochemistry. Images of HaCaT stained with anti- ZO-1 or anti-ZO-2 (green) and counterstained with DAPI (nuclear, blue); quantification of ZO-1 and ZO-2 has been provided in Figure S5 (see supplementary material); scale bar =10 μm. (F) Expression of ZO-1 and ZO-2 in HaCaT cells transfected with either miRIDIAN hsa-miR-146a or hsa-miR-106b mimic or control-mimic for 48 h; data represented as mean ± SD ($n = 4$); $^{*}p < 0.05$ compared to control miRNA mimic. (G) Expression of ZO-1 and ZO-2 in presence of anti-miR to miR-146a and miR-106b inhibitors; data represented as mean ± SD ($n = 4$); $^{*}p < 0.05$ compared to control anti-miR. (H) To test whether ZO-1 or ZO-2 are direct targets of miR-146a or miR-106b, keratinocytes were transfected with pmiR Target-ZO1-3′-UTR or pmiR Target-ZO2-3′-UTR firefly luciferase expression constructs and co-transfected with pRL-TK *Renilla* luciferase expression construct, along with either miR-146a, miR106b or control mimics: I, expression of *ZO-1* and *ZO-2* mRNA in presence of miR-146a and miR-106b mimics; data represented as mean ± SD ($n = 3$); $^{*}p < 0.05$ compared to control transfected cells

but did suppress gene expression by possibly targeting the exonic or 5′-UTR regions of the mRNA [55,56]. The significance of miR-106b is even more poorly understood than that of miR-146a. Recently miR-106b has been causally linked to mitochondrial dysfunction [57], a response that is also known to be implicated in epithelial barrier disruption [58]. Findings of this study lead to the notion that topical delivery of miR-146a and miR-106b inhibitors to the functionally compromised skin produced from biofilm-infected wounds may restore barrier function and secure functional closure of the wound.

When bacteria form a biofilm in the human host, the infection often becomes very resistant to treatment and can contribute to the development of chronic disease. The current literature is equivocal on whether biofilm may compromise wound closure [36,59]. Our model of host response in a chronic wound has enabled the observation that following weeks of biofilm infection, skin barrier function may be compromised. This observation

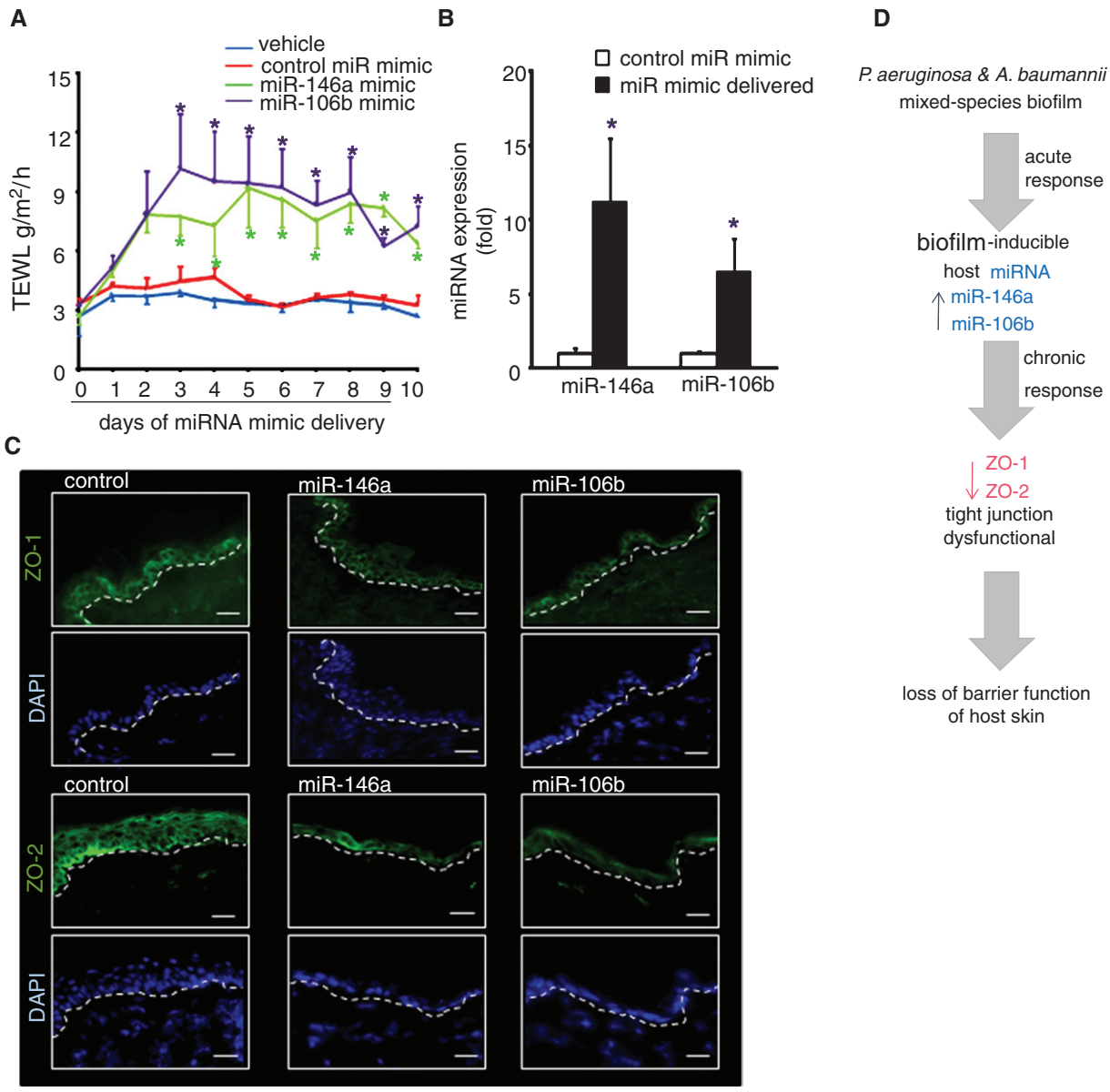

Figure 7. miRNA 146a and miR106b disrupts tight junction proteins in epidermis and increases transepidermal water loss (TEWL) in skin. MiR-146a mimic, miR-106b mimic and non-targeting miRNA mimic (*C. elegans* miR-67 as negative control) were mixed in a cream and applied to a marked area on the dorsal skin of mice for 10 days. TEWL measurements were taken daily, using Dermalab Series Skinlab Combo. The animals were sacrificed at day 11 and the skin where the mimic was applied was harvested for miRNA and immunohistochemistry (IHC) analysis. (A) TEWL analysis of mouse skin following delivery of miR-146a and miR-106b or control mimics; data are mean ± SD ($n = 3$); $^{*}p < 0.05$ compared to mice that received control miRNA mimic. (B) Quantitative real-time PCR of skin where miR-146a and miR-106b mimic was applied; data are mean ± SD ($n = 3$); $^{*}p < 0.05$ compared to mice that received control miRNA mimic. (C) IHC images of mouse skin delivered with miR-146a and miR-106b mimic stained with tight junction proteins ZO-1 and ZO-2 (green) and counterstained with DAPI (blue). The quantification of ZO-1 and ZO-2 has been provided in Figure S6 (see supplementary material). (D) Summary illustration depicting acute-phase induction of biofilm-inducible miRs followed by silencing of *ZO-1* and *ZO-2*, resulting in longer-term compromise of skin barrier function

is particularly clinically significant because it shows that even if a biofilm infected wound visually appeared to be closed, its barrier function may be compromised. Such failed or leaky skin may serve as an open portal, allowing further infection and wound-healing complications. Thus, reliance on functional measures of skin barrier function as a measure in addition to conventional wound inspection seems prudent. Furthermore, wound care may be enhanced by restoration of barrier function of incompletely closed wounds. Another highlight of this work is the recognition of wound biofilm-inducible miR-146a and miR-106b. The observation that wound biofilm may induce host skin miRNAs is novel and particularly significant, because these miRNAs target the same tight junction proteins of the ZO family that are known to be critically required for skin barrier function. The field of post-transcriptional gene silencing of ZO proteins is in its infancy, with miR-212 being the only miR to silence ZO-1. The current report identifies two miRs that silence both ZO-1 and ZO-2, the most

critical ZOs of the three-member ZO family. The observation that biofilms may induce host skin miRNAs to compromise skin function is novel and sets the stage for intervention strategies aimed at inhibiting these miRNAs, with the goal of restoring skin barrier function.

Acknowledgements

Supported by the National Institutes of Health (NIH; Grant Nos GM077185, GM069589 and DOD W81XWH-11-2-0142 to CKS; NIH NR013898 to CKS and DJW; and in part by NIH DK076566 to SR and NIH R01AI097511 to DJW). The funders had no role in study design, data collection and analysis, decision to publish or preparation of the manuscript.

Author contributions

SR, HE, DJW, CHC, GMG and CKS conceived and designed the study; CKS, SR, HE, DJW, HMP, CHC, GMG and VB wrote the manuscript; SR, HE, KG, MS, CM, SK, EM, SC, VB and HMP collected and analysed data for this study and participated in the preparation of the manuscript.

References

1. Sen CK, Gordillo GM, Roy S, *et al.* Human skin wounds: a major and snowballing threat to public health and the economy. *Wound Repair Regen* 2009; **17:** 763–771.
2. Lopez D, Vlamakis H, Kolter R. Generation of multiple cell types in *Bacillus subtilis*. *FEMS Microbiol Rev* 2009; **33:** 152–163.
3. James GA, Swogger E, Wolcott R, *et al.* Biofilms in chronic wounds. *Wound Repair Regen* 2008; **16:** 37–44.
4. Hall-Stoodley L, Costerton JW, Stoodley P. Bacterial biofilms: from the natural environment to infectious diseases. *Nat Rev Microbiol* 2004; **2:** 95–108.
5. Seth AK, Geringer MR, Hong SJ, *et al. In vivo* modeling of biofilm-infected wounds: a review. *J Surg Res* 2012; **178:** 330–338.
6. Watters C, DeLeon K, Trivedi U, *et al. Pseudomonas aeruginosa* biofilms perturb wound resolution and antibiotic tolerance in diabetic mice. *Med Microbiol Immunol* 2013; **202:** 131–141.
7. Watters C, Everett JA, Haley C, *et al.* Insulin treatment modulates the host immune system to enhance *Pseudomonas aeruginosa* wound biofilms. *Infect Immun* 2014; **82:** 92–100.
8. Dalton T, Dowd SE, Wolcott RD, *et al.* An *in vivo* polymicrobial biofilm wound infection model to study interspecies interactions. *PLoS One* 2011; **6:** e27317.
9. Sullivan TP, Eaglstein WH, Davis SC, *et al.* The pig as a model for human wound healing. *Wound Repair Regen* 2001; **9:** 66–76.
10. Gordillo GM, Bernatchez SF, Diegelmann R, *et al.* Preclinical models of wound healing: is man the model? Proceedings of the Wound Healing Society Symposium. *Adv Wound Care (New Rochelle)* 2013; **2:** 1–4.
11. Geyer M, Markou A. The role of preclinical models in the development of psychotropic drugs. In *Neuropsychopharmacology: the Fifth Generation of Progress*, Davis KL (ed.) Lippincott Williams & Wilkins, Philadelphia, 2002; 445–454.
12. Davis SC, Ricotti C, Cazzaniga A, *et al.* Microscopic and physiologic evidence for biofilm-associated wound colonization *in vivo*. *Wound Repair Regen* 2008; **16:** 23–29.
13. Bjarnsholt T. The role of bacterial biofilms in chronic infections. *Acta Pathol Microbiol Immunol Scand* (suppl) 2013: 1–51.
14. Calhoun JH, Murray CK, Manring MM. Multidrug-resistant organisms in military wounds from Iraq and Afghanistan. *Clin Orthop Relat Res* 2008; **466:** 1356–1362.
15. Dallo SF, Weitao T. Insights into *Acinetobacter* war-wound infections, biofilms, and control. *Adv Skin Wound Care* 2010; **23:** 169–174.
16. CMS. Decision memo for electrostimulation for wounds (CAG-00068N), 2002.
17. Holloway BW, Krishnapillai V, Morgan AF. Chromosomal genetics of *Pseudomonas*. *Microbiol Rev* 1979; **43:** 73–102.
18. Roy S, Biswas S, Khanna S, *et al.* Characterization of a preclinical model of chronic ischemic wound. *Physiol Genom* 2009; **37:** 211–224.
19. Elgharably H, Mann E, Awad H, *et al.* First evidence of sternal wound biofilm following cardiac surgery. *PLoS One* 2013; **8:** e70360.
20. Roy S, Patel D, Khanna S, *et al.* Transcriptome-wide analysis of blood vessels laser captured from human skin and chronic wound-edge tissue. *Proc Natl Acad Sci USA* 2007; **104:** 14472–14477.
21. Biswas S, Roy S, Banerjee J, *et al.* Hypoxia inducible microRNA 210 attenuates keratinocyte proliferation and impairs closure in a murine model of ischemic wounds. *Proc Natl Acad Sci USA* 2010; **107:** 6976–6981.
22. Anderson GG, Moreau-Marquis S, Stanton BA, *et al. In vitro* analysis of tobramycin-treated *Pseudomonas aeruginosa* biofilms on cystic fibrosis-derived airway epithelial cells. *Infect Immun* 2008; **76:** 1423–1433.
23. Zhao G, Hochwalt PC, Usui ML, *et al.* Delayed wound healing in diabetic (db/db) mice with *Pseudomonas aeruginosa* biofilm challenge: a model for the study of chronic wounds. *Wound Repair Regen* 2010; **18:** 467–477.
24. Chan YC, Roy S, Khanna S, *et al.* Downregulation of endothelial microRNA-200b supports cutaneous wound angiogenesis by desilencing GATA binding protein 2 and vascular endothelial growth factor receptor 2. *Arterioscler Thromb Vasc Biol* 2012; **32:** 1372–1382.
25. Roy S, Khanna S, Azad A, *et al.* Fra-2 mediates oxygen-sensitive induction of transforming growth factor-β in cardiac fibroblasts. *Cardiovasc Res* 2010; **87:** 647–655.
26. Mehta RC, Stecker KK, Cooper SR, *et al.* Intercellular adhesion molecule-1 suppression in skin by topical delivery of anti-sense oligonucleotides. *J Invest Dermatol* 2000; **115:** 805–812.
27. Parsek MR, Singh PK. Bacterial biofilms: an emerging link to disease pathogenesis. *Annu Rev Microbiol* 2003; **57:** 677–701.
28. Martineau L, Davis SC, Peng HT, *et al.* Controlling methicillin-resistant *Staphyloccocus aureus* and *Pseudomonas aeruginosa* wound infections with a novel biomaterial. *J Invest Surg* 2007; **20:** 217–227.
29. Tredget EE, Shankowsky HA, Groeneveld A, *et al.* A matched-pair, randomized study evaluating the efficacy and safety of Acticoat silver-coated dressing for the treatment of burn wounds. *J Burn Care Rehabil* 1998; **19:** 531–537.
30. Whiteley M, Bangera MG, Bumgarner RE, *et al.* Gene expression in *Pseudomonas aeruginosa* biofilms. *Nature* 2001; **413:** 860–864.
31. Perez-Osorio AC, Williamson KS, Franklin MJ. Heterogeneous *rpoS* and *rhlR* mRNA levels and *16S* rRNA/rDNA (rRNA gene) ratios within *Pseudomonas aeruginosa* biofilms, sampled by laser capture microdissection. *J Bacteriol* 2010; **192:** 2991–3000.
32. Lenz AP, Williamson KS, Pitts B, *et al.* Localized gene expression in *Pseudomonas aeruginosa* biofilms. *Appl Environ Microbiol* 2008; **74:** 4463–4471.
33. Pinnagoda J, Tupker RA, Agner T, *et al.* Guidelines for transepidermal water loss (TEWL) measurement. A report from

the Standardization Group of the European Society of Contact Dermatitis. *Contact Dermatitis* 1990; **22:** 164–178.
34. Pummi K, Malminen M, Aho H, *et al.* Epidermal tight junctions: ZO-1 and occludin are expressed in mature, developing, and affected skin and *in vitro* differentiating keratinocytes. *J Invest Dermatol* 2001; **117:** 1050–1058.
35. Kennedy P, Brammah S, Wills E. Burns, biofilm and a new appraisal of burn wound sepsis. *Burns* 2010; **36:** 49–56.
36. Wolcott RD, Rhoads DD. A study of biofilm-based wound management in subjects with critical limb ischaemia. *J Wound Care* 2008; **17:** 145–148, 150–142, 154–145.
37. Gurjala AN, Geringer MR, Seth AK, *et al.* Development of a novel, highly quantitative *in vivo* model for the study of biofilm-impaired cutaneous wound healing. *Wound Repair Regen* 2011; **19:** 400–410.
38. Kirketerp-Moller K, Jensen PO, Fazli M, *et al.* Distribution, organization, and ecology of bacteria in chronic wounds. *J Clin Microbiol* 2008; **46:** 2717–2722.
39. Furuse M. Molecular basis of the core structure of tight junctions. *Cold Spring Harb Perspect Biol* 2010; **2:** a002907.
40. Kirschner N, Rosenthal R, Gunzel D, *et al.* Tight junctions and differentiation – a chicken or the egg question? *Exp Dermatol* 2012; **21:** 171–175.
41. Hartsock A, Nelson WJ. Adherens and tight junctions: structure, function and connections to the actin cytoskeleton. *Biochim Biophys Acta* 2008; **1778:** 660–669.
42. Monteiro AC, Sumagin R, Rankin CR, *et al.* JAM-A associates with ZO-2, Afadin and PDZ-GEF1 to activate Rap2c and regulate epithelial barrier function. *Mol Biol Cell* 2013; **24**: 2849–2860.
43. Katsuno T, Umeda K, Matsui T, *et al.* Deficiency of zonula occludens-1 causes embryonic lethal phenotype associated with defected yolk sac angiogenesis and apoptosis of embryonic cells. *Mol Biol Cell* 2008; **19:** 2465–2475.
44. Xu J, Kausalya PJ, Phua DC, *et al.* Early embryonic lethality of mice lacking ZO-2, but Not ZO-3, reveals critical and nonredundant roles for individual zonula occludens proteins in mammalian development. *Mol Cell Biol* 2008; **28:** 1669–1678.
45. Ireton K. Molecular mechanisms of cell-cell spread of intracellular bacterial pathogens. *Open Biol* 2013; **3:** 130079.
46. Clark CA, Thomas LK, Azghani AO. Inhibition of protein kinase C attenuates *Pseudomonas aeruginosa* elastase-induced epithelial barrier disruption. *Am J Respir Cell Mol Biol* 2011; **45:** 1263–1271.
47. Yi R, O'Carroll D, Pasolli HA, *et al.* Morphogenesis in skin is governed by discrete sets of differentially expressed microRNAs. *Nat Genet* 2006; **38:** 356–362.
48. Ye D, Guo S, Al-Sadi R, *et al.* MicroRNA regulation of intestinal epithelial tight junction permeability. *Gastroenterology* 2011; **141:** 1323–1333.
49. Yang Y, Ma Y, Shi C, *et al.* Overexpression of miR-21 in patients with ulcerative colitis impairs intestinal epithelial barrier function through targeting the Rho GTPase RhoB. *Biochem Biophys Res Commun* 2013; **434:** 746–752.
50. Tang Y, Banan A, Forsyth CB, *et al.* Effect of alcohol on miR-212 expression in intestinal epithelial cells and its potential role in alcoholic liver disease. *Alcohol Clin Exp Res* 2008; **32:** 355–364.
51. Sonkoly E, Stahle M, Pivarcsi A. MicroRNAs and immunity: novel players in the regulation of normal immune function and inflammation. *Semin Cancer Biol* 2008; **18:** 131–140.
52. Jurkin J, Schichl YM, Koeffel R, *et al.* miR-146a is differentially expressed by myeloid dendritic cell subsets and desensitizes cells to TLR2-dependent activation. *J Immunol* 2010; **184:** 4955–4965.
53. Liu Z, Lu CL, Cui LP, *et al.* MicroRNA-146a modulates TGF-β1-induced phenotypic differentiation in human dermal fibroblasts by targeting SMAD4. *Arch Dermatol Res* 2012; **304:** 195–202.
54. Xu J, Wu W, Zhang L, *et al.* The role of microRNA-146a in the pathogenesis of the diabetic wound-healing impairment: correction with mesenchymal stem cell treatment. *Diabetes* 2012; **61:** 2906–291.
55. Forman JJ, Coller HA. The code within the code: microRNAs target coding regions. *Cell Cycle* 2010; **9:** 1533–1541.
56. Wang WX, Wilfred BR, Xie K, *et al.* Individual microRNAs (miRNAs) display distinct mRNA targeting 'rules'. *RNA Biol* 2010; **7:** 373–380.
57. Zhang Y, Yang L, Gao YF, *et al.* MiR-106b induces mitochondrial dysfunction and insulin resistance in C2C12 myotubes by targeting mitofusin-2. *Mol Cell Endocrinol* 2013; **381**: 230–240.
58. Ma C, Wickham ME, Guttman JA, *et al. Citrobacter rodentium* infection causes both mitochondrial dysfunction and intestinal epithelial barrier disruption *in vivo*: role of mitochondrial associated protein (Map). *Cell Microbiol* 2006; **8:** 1669–1686.
59. Thomson CH. Biofilms: do they affect wound healing? *Int Wound J* 2011; **8:** 63–67.

SUPPLEMENTARY MATERIAL ON THE INTERNET

The following supplementary material may be found in the online version of this article:

Supplementary materials and methods

Figure S1. Establishment of full-thickness preclinical porcine burn model

Figure S2. Persistent infection in inoculated burn wounds

Figure S3. Haematoxylin and eosin-stained sections related to Figure 5A

Figure S4. Bioinformatics prediction for miR-146a and miR-106b targeting 3′-UTR of ZO-1 and ZO-2

Figure S5. Quantification of ZO-1 and ZO-2 signals related to Figure 6E

Figure S6. Quantification of ZO-1 and ZO-2 signals in Figure 7C